Research Square

Preprints are preliminary reports that have not undergone peer review.
They should not be considered conclusive, used to inform clinical practice,
or referenced by the media as validated information.

Spatiotemporal Dynamics of Vegetation NPP and Its Lagged and Cumulative Responses to Climatic Factors in the Qinba Mountains

Feng Xu
Xinyang Normal University, Xinyang
Xin Yao
Xinyang Normal University, Xinyang
Fangyuan Huang
Xinyang Normal University, Xinyang
Shaomian Niu
Xinyang Normal University, Xinyang
Liyang Liu
Xinyang Normal University, Xinyang
Shouye Liu
Xinyang Normal University, Xinyang
JiQiang Niu
niujiqiang@xynu.edu.cn

Xinyang Normal University, Xinyang

Article

Keywords: Qinba Mountains, monthly-scale dynamics, driving mechanisms, lagged and cumulative effects

Posted Date: July 20th, 2026

DOI: https://doi.org/10.21203/rs.3.rs-10250080/v1

License: This work is licensed under a Creative Commons Attribution 4.0 International License.
Read Full License

Additional Declarations: No competing interests reported.

Spatiotemporal Dynamics of Vegetation NPP and Its Lagged and Cumulative Responses to Climatic Factors in the Qinba Mountains

Feng Xu[1,2], Xin Yao[1], Fangyuan Huang[1], Shaomian Niu[1], Liyang Liu[1], Shouye Liu[1], and JiQiang Niu[1,2*]

[1]School of Geographic Sciences, Xinyang Normal University, Xinyang, 464000, China

[2]Henan Key Laboratory for Synergistic Prevention of Water and Soil Environmental Pollution, Xinyang Normal University, Xinyang 464000, China

*Correspondence: niujiqiang@xynu.edu.cn

Abstract: Understanding monthly dynamics and driving mechanisms of vegetation net primary productivity (NPP) is crucial for predicting ecosystem responses to climate change. However, such fine-temporal-scale studies remain limited in the Qinba Mountains (QBMs), a climate-sensitive ecological transition zone in China. Therefore, this study constructed a fine-temporal-scale analytical framework for vegetation NPP dynamics. Using MODIS NPP data (2001–2024), we analyzed the spatiotemporal dynamics of monthly NPP in the QBMs and identified its dominant drivers using XGBoost–SHAP. The lagged and cumulative effects of key climatic factors were further examined. The findings are as follows: (1) temporally, monthly NPP showed a stable seasonal rhythm and continuous increase. Spatially, monthly vegetation NPP underwent a transition from a northwest-low and southeast-high pattern to a northwest-high and southeast-low pattern before gradually returning to the initial spatial configuration. (2) dominant drivers changed across months, with February, June, September, and November as key transition nodes. Specifically, solar radiation (Rad) exceeded soil temperature (Tsoil) in February. Tsoil shifted from positive to negative in June, with increased precipitation (Pre) contribution. Pre and land cover strengthened in September; and Rad regained dominance in November. (3) lagged and cumulative effects differed significantly among climatic factors: temperature (Tem) was dominated by a 3-month lag effect (21.02%), Pre by a 1-month cumulative effect (26.49%), and Rad by a 2-month cumulative effect (46.93%). These findings highlight the importance of monthly-scale analysis for capturing dynamic shifts in limiting factors and provide a scientific basis for ecosystem management and carbon sink enhancement in climate-sensitive ecological transition zones.

Keywords: Qinba Mountains; monthly-scale dynamics; driving mechanisms; lagged and cumulative effects

1. Introduction

Increasing global carbon emissions have intensified the greenhouse effect and profoundly affected terrestrial ecosystems worldwide[1]. As a fundamental component of terrestrial ecosystems, vegetation plays a vital role in maintaining habitable environmental conditions and regulating the global carbon cycle[2]. Among various ecological indicators, vegetation net primary productivity (NPP) has been widely recognized as a key metric for assessing ecosystem sustainability and carbon cycling processes[3]. NPP is generally defined as the amount of organic matter accumulated by vegetation through photosynthesis per unit time after subtracting carbon losses from plant respiration[4,5].

With the rapid development of remote sensing technology and the growing understanding of ecosystem processes and mechanisms, monitoring, estimating, and analyzing the spatiotemporal dynamics of NPP using remote sensing data and estimation models have become important research approaches[6,7]. Existing studies have mainly focused on two aspects: first, analyzing the spatiotemporal trends and future projections of regional NPP[8,9], and second, investigating the effects of climate change and human activities on vegetation NPP[10,11]. In terms of temporal scale, annual-scale studies remain the most common, mainly emphasizing long-term NPP trends, the evolution of spatial patterns, and their responses to climate change and land-use change[9,12]. For example, Xuan and Rao systematically analyzed the spatiotemporal variations and influencing factors of NPP in the middle reaches of the Yellow

River based on MODIS NPP, meteorological, and land-use data from 2000 to 2020, revealing an overall increase in regional NPP and significant spatial heterogeneity[12]. Liu et al. evaluated the spatiotemporal dynamics of annual NPP and its climatic controls at the national grassland scale based on data from 1982 to 2016, indicating that the responses of grassland NPP to climate change varied substantially across regions[13]. Meanwhile, increasing attention has been paid to seasonal-scale variations in NPP, particularly differences in vegetation growth among seasons and the regulatory effects of seasonal climatic factors on NPP[13,14]. Ma et al. demonstrated that the response of NPP to climate change exhibits marked seasonal heterogeneity. Increased precipitation in summer and autumn generally promotes grassland NPP, whereas higher maximum summer temperature may exert an inhibitory effect[14]. Han et al. further found in the Loess Plateau that the effects of vegetation phenological changes on NPP differ substantially among seasons. An earlier start and delayed end of the growing season separately contributed to increases in spring and autumn NPP, whereas summer NPP declined in some arid and semi-arid regions[15]. Compared with annual-scale studies, seasonal-scale analyses can more effectively reveal the stage-specific characteristics of vegetation productivity responses to environmental change[14,15].

However, both annual and seasonal-scale studies are generally based on data with relatively coarse temporal resolutions, which makes it difficult to effectively capture inter-monthly fluctuations, abrupt transition points, and monthly differences in driving factors during vegetation growth[16,17]. The responses of NPP to climate change are highly uncertain across different temporal scales[18,19]. Although existing studies have extensively analyzed NPP variations and their driving factors at annual and seasonal scales, and have partly revealed the effects of climate change and human activities, systematic and quantitative understanding remains limited. Key gaps remain in the monthly-scale shifts of driving factors, the intra-growing-season differences in their effects, and their temporal effects[20,21]. This limitation restricts a deeper understanding of the mechanisms underlying fine-scale dynamic changes in NPP[22].

The Qinba Mountains (QBMs) constitute an important transitional zone along the geographical boundary between northern and southern China[23,24]. This region shapes pronounced north–south environmental differentiation and plays a key ecological role in linking the eastern plains of China with the Qinghai–Tibet Plateau[24]. As a core water conservation area for the Middle Route of the South-to-North Water Diversion Project and a key national corridor for biodiversity conservation, dynamic changes in vegetation productivity in the QBMs have important implications for the national carbon sink pattern[25,26]. Previous studies have shown that vegetation NPP in the QBMs is closely associated with the cumulative temporal effects of drought[27], and the contributions of extreme climate indices to NPP exhibit clear directional differences[28]. However, systematic studies on the spatiotemporal differentiation of monthly NPP and the monthly variability in driving mechanisms in the QBMs remain limited, particularly with respect to the quantitative assessment of the temporal effects of major driving factors during the growing season.

Given these considerations, this study focuses on the QBMs and systematically conducts the following three analyses based on monthly vegetation NPP data from 2001 to 2024: (1) revealing the spatiotemporal differentiation characteristics of monthly NPP in the QBMs from 2001 to 2024, and quantitatively analyzing the evolution of its spatial patterns and long-term trends in monthly NPP; (2) identifying the dominant driving factors of NPP in each month and their dynamic shifts based on the XGBoost–SHAP machine learning framework; and (3) quantifying the lagged and cumulative effects of key climatic factors on NPP during the growing season.

2. Study Area and Datasets

2.1 Study area

The QBMs (30°–36°N, 102°–114°E) are located in the transitional zone between the warm temperate and subtropical regions of central China[29,30]. They form the watershed between the Yellow River Basin and the Yangtze River Basin (Figure 1) and serve as an important ecological corridor connecting eastern and western China[30,31]. The study area covers 30 administrative units across six provinces and municipalities, including Shaanxi, Henan, Hubei,

Chongqing, Sichuan, and Gansu, with a total area of approximately 3.06 × 10^5 km^2[31,32]. The QBMs collectively comprise the Qinling Mountains and the Daba Mountains[29,31]. The Qinling Mountains extend across central China from the Jialing River in the west to the Funiu Mountains in the east, spanning approximately 800 km. The Daba Mountains stretch from the Jialing River Basin in the west to the Wudang Mountains in the east and constitute a natural barrier between southern Shaanxi and northern Sichuan. The region is characterized by a mild and humid climate, with annual precipitation ranging from 700 to 1000 mm and a mean annual temperature of 12–15.7°C[29]. Owing to the combined effects of the north–south transition in hydrothermal conditions and mountain vertical zonation, the QBMs support diverse vegetation types with pronounced transitional characteristics[33-35]. The dominant vegetation types include warm-temperate deciduous broad-leaved forests, northern subtropical evergreen–deciduous broad-leaved mixed forests, mixed coniferous and broad-leaved forests, shrublands, and grasslands[33-35]. Specifically, deciduous broad-leaved forests are mainly distributed in the northern part of the region and in low- to mid-elevation mountainous areas. Evergreen–deciduous broad-leaved mixed forests are primarily found in the southern mountains and low- to mid-elevation areas on south-facing slopes. Mixed coniferous and broad-leaved forests are mostly distributed in mid-mountain zones. Shrublands and grasslands mainly occur in high-elevation areas. Cropland is the dominant land-use type in river valleys, basins, and plains[32,35].

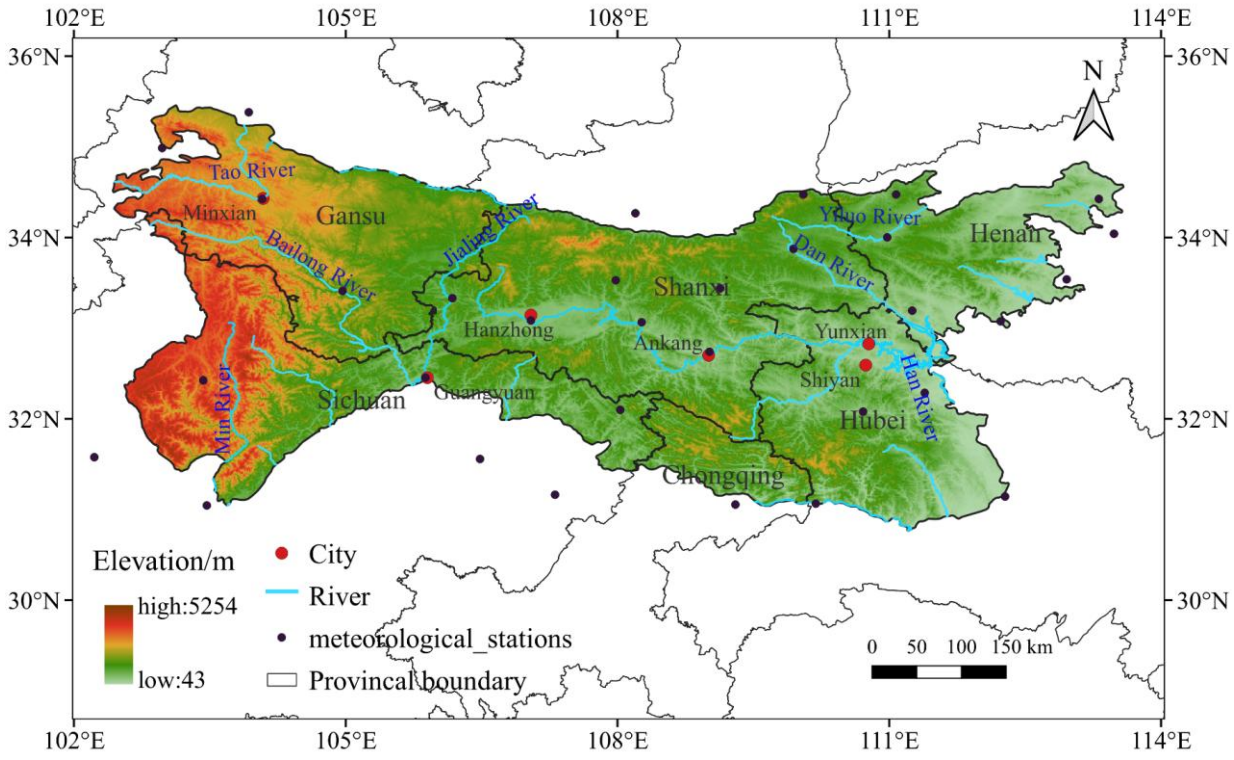


Figure 1. Geographical location of the QBMs

2.2 Data Sources

To analyze the spatiotemporal evolution of monthly vegetation NPP in the QBMs and its responses to environmental factors, this study selected multi-source datasets, including vegetation NPP, climatic factors, topographic factors, and land-cover data.

The vegetation NPP data were derived from the MODIS MOD17A2HGF Version 6.1 product released by NASA (National Aeronautics and Space Administration). This product provides 8-day composite GPP (gross primary productivity) and PsnNet (net photosynthesis) data. The PsnNet band represents net photosynthesis after subtracting maintenance respiration from GPP and can be used to approximate vegetation net productivity. In this study, the PsnNet band was selected and temporally aggregated to generate monthly NPP data.

The climatic factors included temperature, precipitation, soil temperature, soil moisture, and solar radiation,

which were used to examine the responses of vegetation NPP to regional hydrothermal conditions, soil moisture status, and surface energy conditions. Temperature and precipitation data were obtained from the Resource and Environment Science and Data Center of the Chinese Academy of Sciences (RESDC), while soil temperature, soil moisture, and solar radiation data were obtained from the ERA5-Land reanalysis dataset.

The topographic factors included DEM, slope, and aspect, and land-cover data were also used to characterize the effects of terrain conditions and land-cover types on the spatial differentiation of vegetation NPP. These datasets were derived from the Shuttle Radar Topography Mission (SRTM) digital elevation dataset and the China Land Cover Dataset (CLCD) released by Wuhan University, respectively. The names, abbreviations, original temporal resolutions, spatial resolutions, and sources of all datasets are listed in Table 1.

Table 1. Basic information on the datasets used in this study.

Data	Abbreviation	Original temporal resolution	Original spatial resolution	Source
Net Primary Productivity	NPP	day	500 m	NASA (https://www.earthdata.nasa.gov/)
Elevation	Dem	year	30 m	NASA/CGIAR (https://srtm.csi.cgiar.org/)
Landcover type	LC	year	30 m	CLCD (https://doi.org/10.5281/znodo.4417810)
Temperature	Tem	month	1 km	RESDC (https://www.resdc.cn/)
Precipitation	Pre	month	1 km	
Soil temperature	Tsoil	month	0.1°	ECMWF (https://cds.climate.copernicus.eu/)
Soil moisture	SM	month	0.1°	
Solar radiation	Rad	month	0.1°	

3. Methods

The research framework of this study consists of four main components (Figure 2): data preprocessing (see Section 3.1), characterization of the spatiotemporal differentiation of monthly NPP in the QBMs (see Section 3.2), identification of the dominant driving factors of monthly NPP and their dynamic transition patterns (see Section 3.3), and assessment of the lagged and cumulative responses of vegetation NPP to climatic factors (see Section 3.4).

3.1 Data Preprocessing

First, the 8-day PsnNet band data from the MOD17A2HGF product were obtained using the Google Earth Engine (GEE) platform. These data were temporally aggregated by month to generate monthly NPP datasets. Non-vegetated areas and abnormal values were then removed, and consistency preprocessing was performed for the meteorological, topographic, and land-cover datasets. Based on the DEM data, topographic factors, such as, slope and aspect were derived, and all datasets were masked and clipped according to the boundary of the study area. Subsequently, all datasets were projected to the WGS 1984 UTM Zone 50N coordinate system and resampled to a spatial resolution of 1 km to ensure spatial consistency among multi-source datasets. Through the above procedures, monthly NPP, meteorological factors, topographic factors, and land-cover datasets for the study area were finally constructed (see Figure 2).

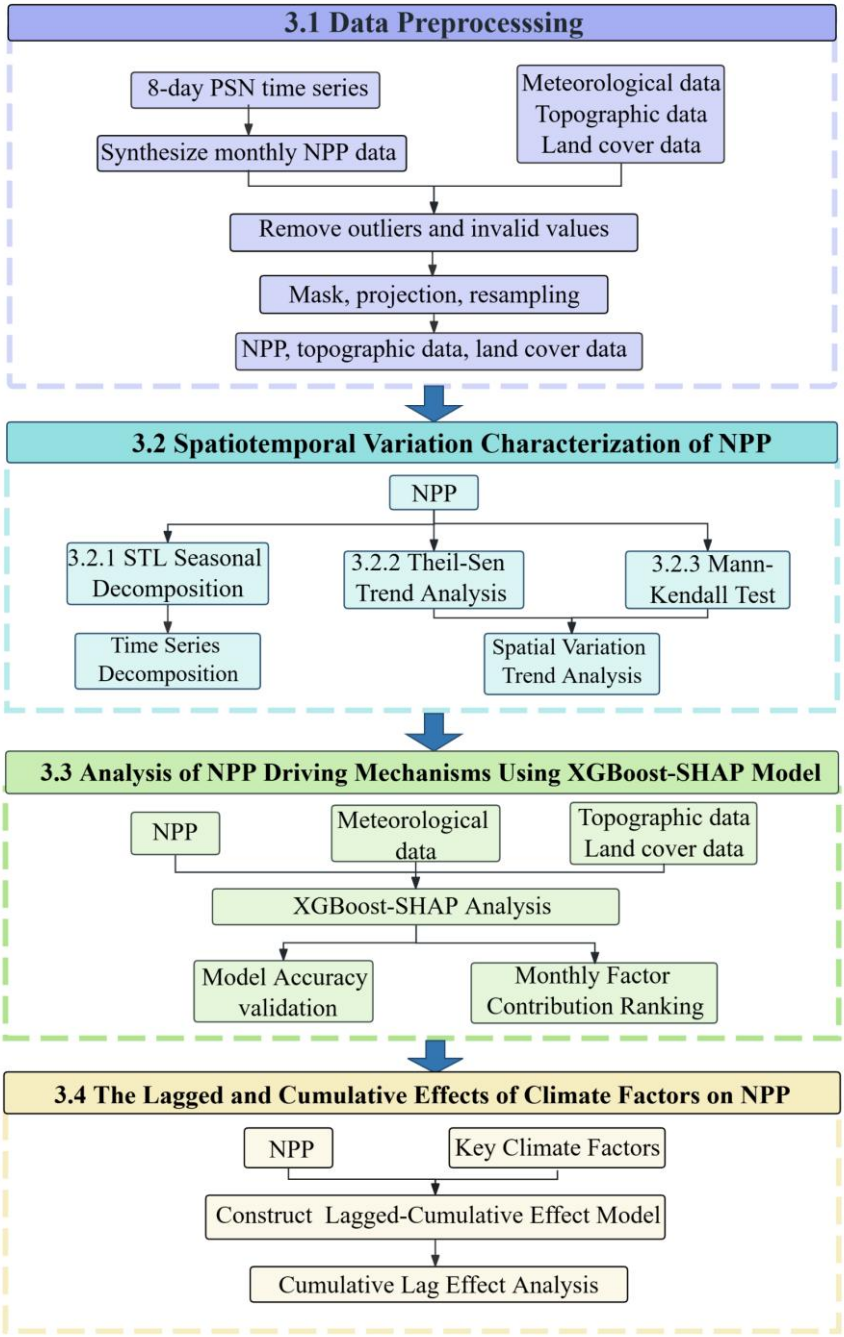


Figure 2. Technical workflow of this study.

3.2 Spatiotemporal Variation Characterization of NPP

3.2.1 STL Seasonal Decomposition

To analyze the temporal variation characteristics of monthly vegetation NPP in the QBMs, this study employed the STL (Seasonal and Trend decomposition using Loess) seasonal decomposition method (see Figure 2). STL is a robust nonparametric statistical method that decomposes an original time series into trend, seasonal, and remainder components, thereby characterizing long-term trends, periodic fluctuations, and random disturbances[36,37]. In this study, STL decomposition was applied to the monthly mean NPP values from January to December over the 24-year period from 2001 to 2024. The decomposition procedure is summarized as follows:

$$Y_t = T_t + S_t + R_t \quad (1)$$

where Y_t denotes the monthly NPP time series from 2001 to 2024, T_t represents the trend component, S_t represents the seasonal component, and R_t represents the residual component. STL decomposition extracts the

trend and seasonal components separately through iterative locally weighted regression smoothing, while reducing the influence of outliers on the decomposition results under a robust regression framework. The iterative procedure can be summarized as follows:

$$\hat{T}_t = \mathrm{Loess}_{\mathrm{trend}}(y_t - \hat{S}_t) \quad (2)$$

$$\hat{S}_t = \mathrm{Loess}_{\mathrm{seasonal}}(y_t - \hat{T}_t) \quad (3)$$

$$\hat{R}_t = y_t - \hat{T}_t - \hat{S}_t \quad (4)$$

where $\mathrm{Loess}_{\mathrm{trend}}$ denotes the smoothing procedure used to extract the long-term trend component, and $\mathrm{Loess}_{\mathrm{seasonal}}$ denotes the smoothing procedure used to extract the seasonal fluctuation component[38]. To quantify the explanatory capacity of the trend and seasonal components for the original time series, trend strength and seasonal strength were calculated, respectively[39,40]:

$$F_T = max\left\{0,1 - \frac{\mathrm{Var}(R_t)}{\mathrm{Var}(NPP - S_t)}\right\} \quad (5)$$

$$F_S = max\left\{0,1 - \frac{\mathrm{Var}(R_t)}{\mathrm{Var}(NPP - T_t)}\right\} \quad (6)$$

here, F_T represents the strength of the trend component. Higher values of F_T indicate that the residual variation after detrending accounts for a smaller proportion of the total variance, implying a more pronounced trend signal. Similarly, F_S measures the strength of the seasonal component, with higher values corresponding to stronger seasonal fluctuations.

3.2.2 Theil–Sen Median Trend Analysis

To assess whether monthly vegetation NPP exhibited increasing or decreasing spatial trends, the Theil–Sen median trend estimator was applied (see Figure 2). The Theil–Sen median trend estimator is a robust nonparametric statistical method for trend analysis that is insensitive to outliers and data noise, making it suitable for analyzing time-series trends with non-normal distributions or outliers. Compared with ordinary least-squares linear regression, the Theil–Sen method is more resistant to the influence of extreme values and is therefore well suited for trend estimation of NPP time series[41]. The basic principle of this method is to calculate the slope between every pair of observations in a time series and then use the median of all pairwise slopes as the overall trend of the series[42]. In this study, a pixel-by-pixel analysis was conducted to construct Sen's slope models for monthly NPP sequences from January to December during 2001–2024, thereby revealing the evolutionary patterns of vegetation productivity across different months. The calculation formula is as follows:

$$S_{NPP} = Median\left(\frac{NPP_j - NPP_i}{j - i}\right) \quad (7)$$

here, NPP_i and NPP_j correspond to the NPP values of a given pixel in the same month of the *i*-th and *j*-th years in the time series, respectively. When $S_{NPP} > 0$, the monthly NPP exhibits an increasing trend over the study period, indicating improved vegetation growth conditions. When $S_{NPP} < 0$, the monthly NPP exhibits a decreasing trend over the study period, suggesting that vegetation growth may have been suppressed or degraded.

3.2.3 Mann–Kendall Test

To determine whether the spatial trends in NPP were statistically significant, the Mann–Kendall test was applied (see Figure 2). As a nonparametric statistical method, the Mann–Kendall test is widely used to detect the significance of monotonic trends in time series without requiring the data to follow a normal distribution[43-45]. The Mann–Kendall test statistic is calculated as follows:

$$Z = \begin{cases} \dfrac{S-1}{\sqrt{Var(S)}}, & |S| > 0 \\ 0, & S = 0 \\ \dfrac{S+1}{\sqrt{Var(S)}}, & |S| < 0 \end{cases} \quad (8)$$

$$S = \sum_{i=1}^{n-1} \sum_{j=i+1}^{n} sgn\left(NPP_j - NPP_i\right) \tag{9}$$

$$sgn\left(NPP_j - NPP_i\right) = \begin{cases} 1 \cdot if\ NPP_j - NPP_i > 0 \\ 0 \cdot if\ NPP_j - NPP_i = 0 \\ -1 \cdot if\ NPP_j - NPP_i < 0 \end{cases} \tag{10}$$

$$Var(S) = \frac{n(n-1)(2n+5) - \sum_{i=1}^{m} t_i(t_i-1)(2t_i+5)}{18} \tag{11}$$

where, NPP_i and NPP_j represent the NPP values of a given pixel in the corresponding month of the *i*-th and *j*-th years, respectively. n denotes the length of the time series, with n = 24 in this study, m represents the number of tied groups, sgn is the sign function, and the statistic Z ranges from (-∞, +∞). When $|Z| < 1.65$, the trend is considered nonsignificant. When ($1.65 \leq |Z| < 1.96$), the trend passes the 90% significance test and is classified as a weakly significant change. When ($1.96 \leq |Z| < 2.58$), the trend passes the 95% significance test and is classified as a significant change. When ($|Z| \geq 2.58$), the trend passes the 99% significance test and is classified as a highly significant change. By combining the direction of the Theil–Sen slope, NPP trends were further classified into seven categories: nonsignificant increase, significant increase, highly significant increase, no change, nonsignificant decrease, significant decrease, and highly significant decrease.

3.3 Analysis of NPP Driving Mechanisms Using XGBoost–SHAP

To quantify the nonlinear responses of vegetation NPP to climatic factors and human activities in the QBMs, an Extreme Gradient Boosting (XGBoost) regression model was constructed (see Figure 2). XGBoost is an ensemble learning algorithm proposed by Chen. It does not require assumptions about data distribution and can capture complex nonlinear relationships and high-order interactions while reducing overfitting through regularization[46]. To improve model interpretability, the SHAP method was further used for attribution analysis[47] (see Figure 2). SHAP calculates the Shapley value of each feature to quantify its contribution to model predictions and decomposes the predicted NPP into a baseline value and feature-specific attribution values. The global dominant factors of NPP variation were identified using the mean absolute SHAP values. In addition, nonlinear response thresholds and positive–negative effect transitions between key drivers, such as temperature and precipitation, and NPP were analyzed.

3.4 The Lagged and Cumulative Effects of Climate Factors on NPP

To analyze differences in the climatic responses of vegetation NPP in the QBMs, monthly temperature, precipitation, soil temperature, and solar radiation were selected as climatic factors (see Figure 2). Vegetation NPP was used as the dependent variable, and linear regression was established to assess the effects of each climatic factor on NPP under different cumulative and lagged conditions[48]. Previous studies have shown that vegetation responses to climate change usually exhibit monthly-scale time effects[19,48,49], with lag times mostly occurring within one quarter. Therefore, the cumulative and lagged periods of climatic factors were both set to 0–3 months in this study. Taking a climatic factor X as an example, its temporal effect on current-month NPP can be expressed as follows:

$$NPP_t = b \sum_{j=0}^{m} X_{t-n-j} + a \tag{12}$$

where NPP_t denotes vegetation NPP in month t, X_{t-n-j} represents the value of the climatic factor at the j-th month within the cumulative period prior to month t, after applying a lag of n months, a and b are the intercept and regression coefficient, respectively, while m and n denote the cumulative and lag time scales, respectively. Following Ding et al., both m and n were constrained to range from 0 to 3, with a sum of[48]. Accordingly, ten temporal-effect scenarios were defined in this study: no temporal effect (m = 0, n = 0), 1–3-month lag effects (m = 0, n = 1, 2, 3), 1–3-month cumulative effects (m = 1, 2, 3; n = 0), a 1-month cumulative effect with a 1-month

lag ($m = 1$, $n = 1$), a 2-month cumulative effect with a 1-month lag ($m = 2$, $n = 1$), and a 1-month cumulative effect with a 2-month lag ($m = 1$, $n = 2$)[50]. For each climatic variable, regression models were established under the ten temporal-effect scenarios, and the scenario with the highest coefficient of determination R^2 was identified as the optimal temporal effect of that climatic factor on NPP[20]. For example, if the model constructed using NPP from March to October during 2001–2024 and precipitation from January to July of the corresponding years yields the highest R^2 for a given pixel, this indicates that the effect of precipitation on NPP at that pixel exhibits a temporal response, with the optimal form being a 3-month lag effect. Using the same procedure, the optimal cumulative and lag time scales of each climatic factor affecting NPP can be further identified at the pixel scale. It should be noted that when $m = 0$ and $n = 0$, the climatic factor exerts only an instantaneous effect on NPP in the current month, with no cumulative or lagged effect. When $m > 0$ and $n = 0$, only a cumulative effect is present. when $m = 0$ and $n > 0$, only a lagged effect is present, and when $m > 0$ and $n > 0$, both cumulative and lagged effects are present.

4. Results

4.1 Spatiotemporal Changes in Vegetation NPP

To identify the long-term trends, periodic variations, and random fluctuations in the monthly NPP time series of the QBMs, the STL seasonal decomposition method described in Section 3.2.1 was applied to the monthly NPP series from 2001 to 2024 (Figure 3). The trend component showed an overall increasing trend during the study period, with a fitted slope of 0.04 (trend strength = 0.12) (Figure 3a). The seasonal component exhibited a stable intra-annual cycle, with the peak consistently occurring in July (seasonal strength = 0.95) (Figure 3b). The residual component fluctuated around zero and showed no obvious long-term trend (Figure 3c).

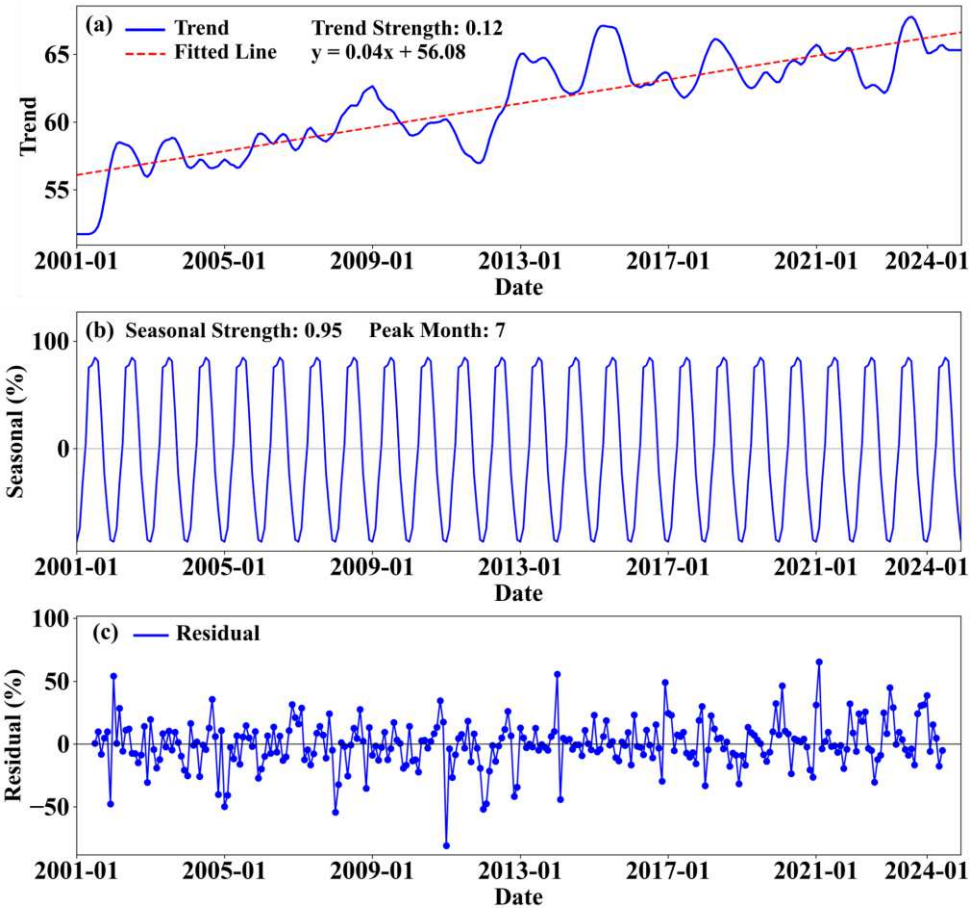


Figure 3. STL seasonal decomposition results of the monthly vegetation NPP time series in the QBMs: panels (a), (b), and (c) represent the trend, seasonal, and residual components derived from STL decomposition.

The interannual trend analysis for each month revealed distinct variations in the long-term dynamics of monthly NPP in the QBMs (Figure 4). From 2001 to 2024, the direction and magnitude of NPP trends varied among different months. April and May showed the highest increasing rates, with slopes of 1.12 and 1.02 g C m^{-2} yr^{-1}, respectively, indicating rapid increases in NPP during these months. After June, the increasing rate gradually declined. NPP still showed an increasing trend in July (slope = 0.35 g C m^{-2} yr^{-1}), whereas August exhibited a decreasing trend (slope = −0.12 g C m^{-2} yr^{-1}). The remaining months generally showed increasing trends, but with relatively small changes. For example, the slopes in January, February, and December were 0.19, 0.30, and 0.23 g C m^{-2} yr^{-1}, respectively.

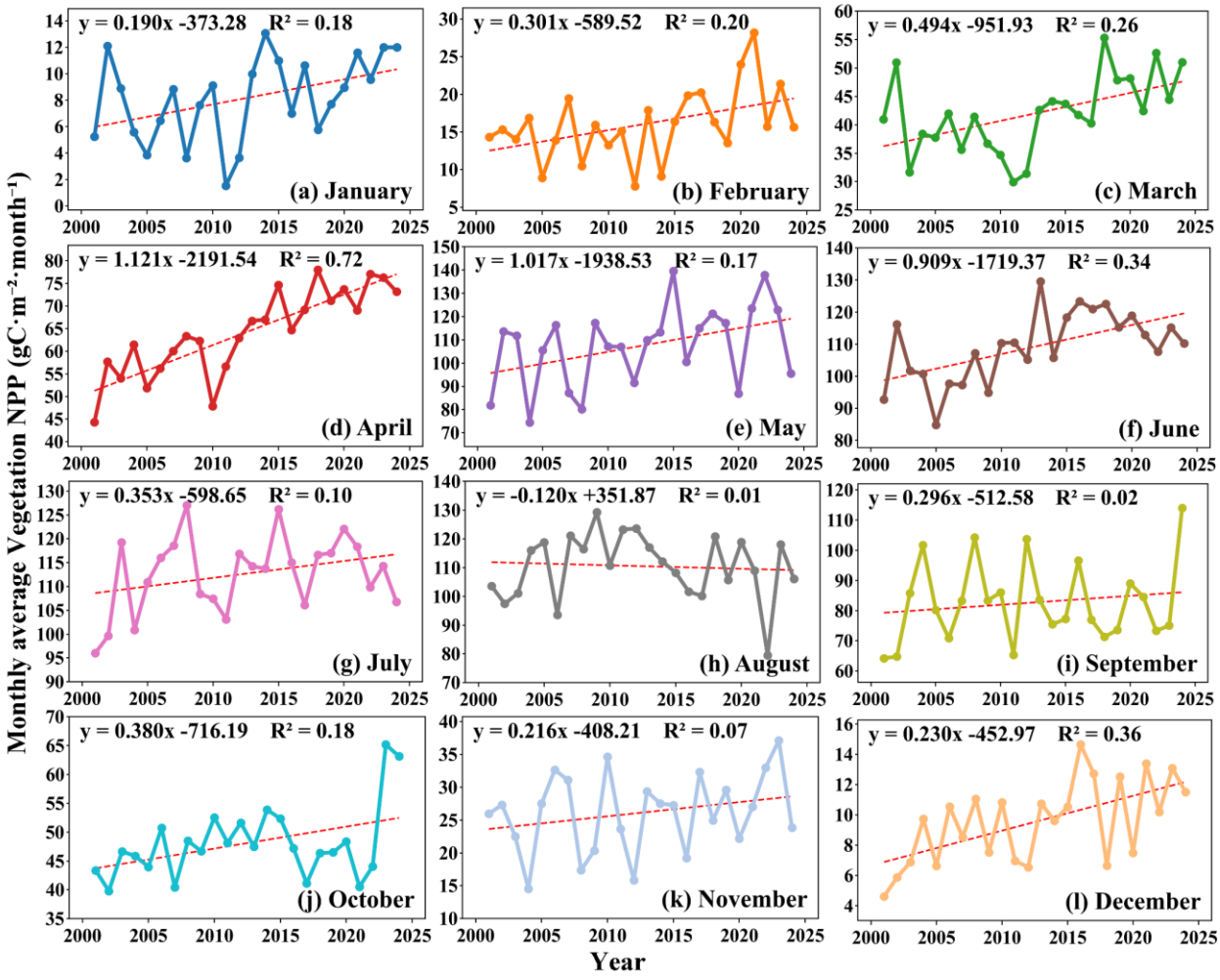


Figure 4. Monthly NPP trends in the QBMs from 2001 to 2024. Panels (a)–(l) represent January–December, respectively; red dashed lines show fitted trends.

Monthly NPP in the QBMs showed clear intra-annual variations from January to December (Figure 5, Table 2). NPP gradually increased from January and exhibited a spatial pattern of lower values in the northwest and higher values in the southeast during January–April. High-value areas were mainly distributed in the southern Daba Mountains, Shennongjia, and the southeastern mountainous regions. During May–August, NPP reached a high level, with regional mean values ranging from 107.38 to 112.68 g C m^{-2} $month^{-1}$ and peaking in July (112.68 g C m^{-2} $month^{-1}$). Meanwhile, high-value areas shifted toward the western high-elevation regions and northern mountains, while the Hanjiang Basin and Ankang Basin became relatively low-value areas. After September, NPP declined gradually, and the spatial pattern returned to that observed during January–April by November–December. The CV values were higher in January and December (78.73% and 76.17%, respectively) but lowest in September (25.21%), indicating stronger spatial heterogeneity during low-NPP months. Overall, the western high-elevation regions exhibited

the most pronounced monthly variations, whereas the southern Daba Mountains, Shennongjia, and southeastern mountainous regions maintained relatively high NPP values throughout most months.

Table 2. Spatial statistical characteristics of monthly average NPP in the QBMs, 2001–2024

Month	Mean	Median	Min	Max	SD	CV (%)
January	8.15	7.40	-4.33	44.17	6.42	78.73
February	15.98	16.48	-1.89	64.35	9.98	62.44
March	41.91	44.88	-0.22	130.04	20.50	48.91
April	64.15	71.99	0.03	155.67	26.28	40.97
May	107.38	110.59	1.16	257.53	36.19	33.70
June	109.15	107.02	-58.47	296.56	39.13	35.85
July	112.68	109.97	-38.73	319.75	40.98	36.37
August	110.51	109.50	-34.38	276.72	32.53	29.44
September	82.69	83.70	4.43	181.30	20.85	25.21
October	48.11	53.63	0.56	109.49	19.39	40.30
November	26.11	25.94	0.13	91.10	14.35	54.94
December	9.53	8.70	-4.36	49.53	7.26	76.17

Note: Mean, Median, Min, Max, and SD represent the mean, median, minimum, maximum, and standard deviation, respectively, all in g C m^{-2} $month^{-1}$; CV represents the coefficient of variation, where CV = SD / Mean × 100%, in %.

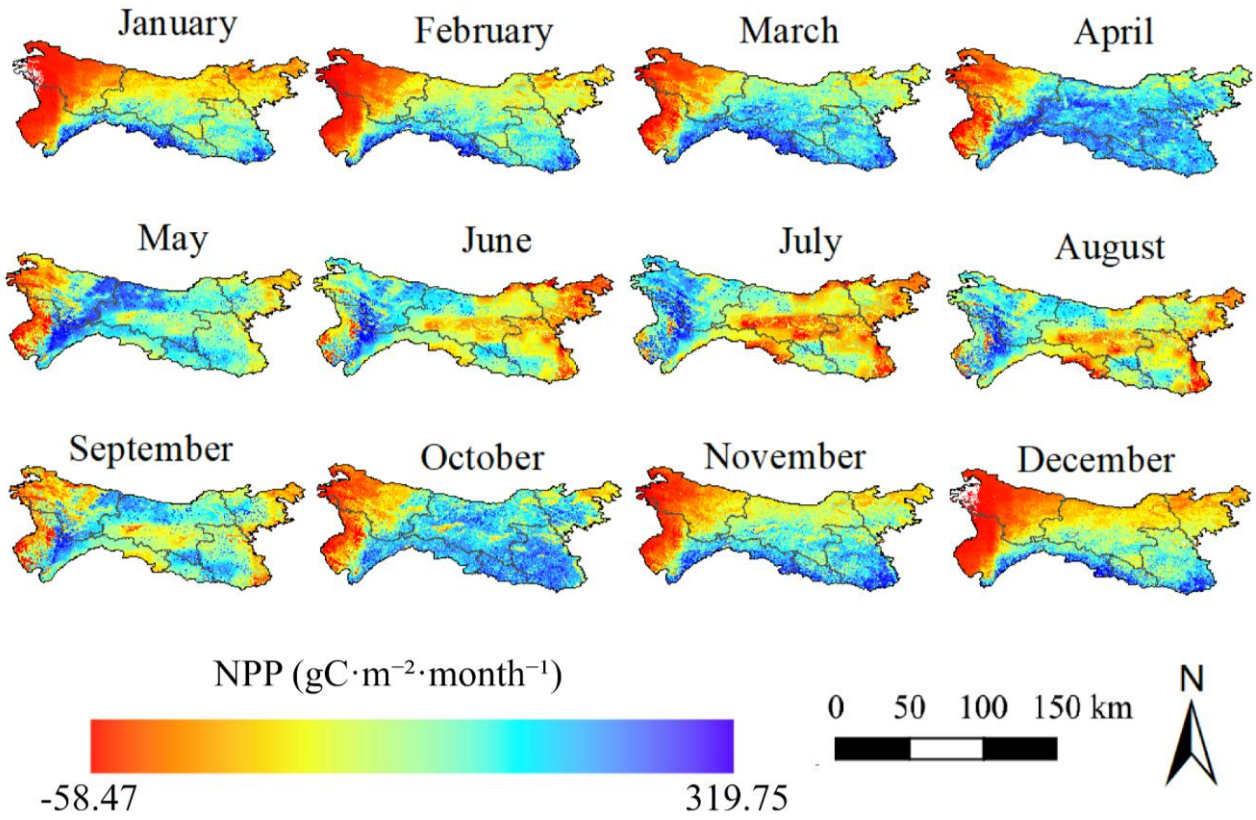


Figure 5. Spatial distribution of monthly mean vegetation NPP in the QBMs during 2001–2024.

The spatial trends of monthly NPP in the QBMs were further analyzed using the Theil–Sen trend analysis and Mann–Kendall significance test methods described in Sections 3.2.2 and 3.2.3 (Figure 6). Results showed clear monthly differences and spatial heterogeneity in NPP trends during 2001–2024. Except for August, all months showed overall increasing trends. The areas with increasing trends accounted for 87.88%–96.46% from December

to June. April exhibited the most concentrated increase, with strongly significant increasing areas accounting for 65.99%, mainly distributed on the southern slope of the Qinling Mountains, the Daba Mountains, and Shennongjia. From July to September, decreasing trends expanded, with the largest proportion occurring in August (59.59%), mainly distributed in the central and eastern regions and some basin areas. Increasing trends recovered in October and November, accounting for 85.82% and 83.25%, respectively. Overall, monthly NPP trends in the QBMs were dominated by increases, while decreasing trends became more pronounced during July–September, especially in August, indicating strong monthly variations in the spatial patterns of NPP trends.

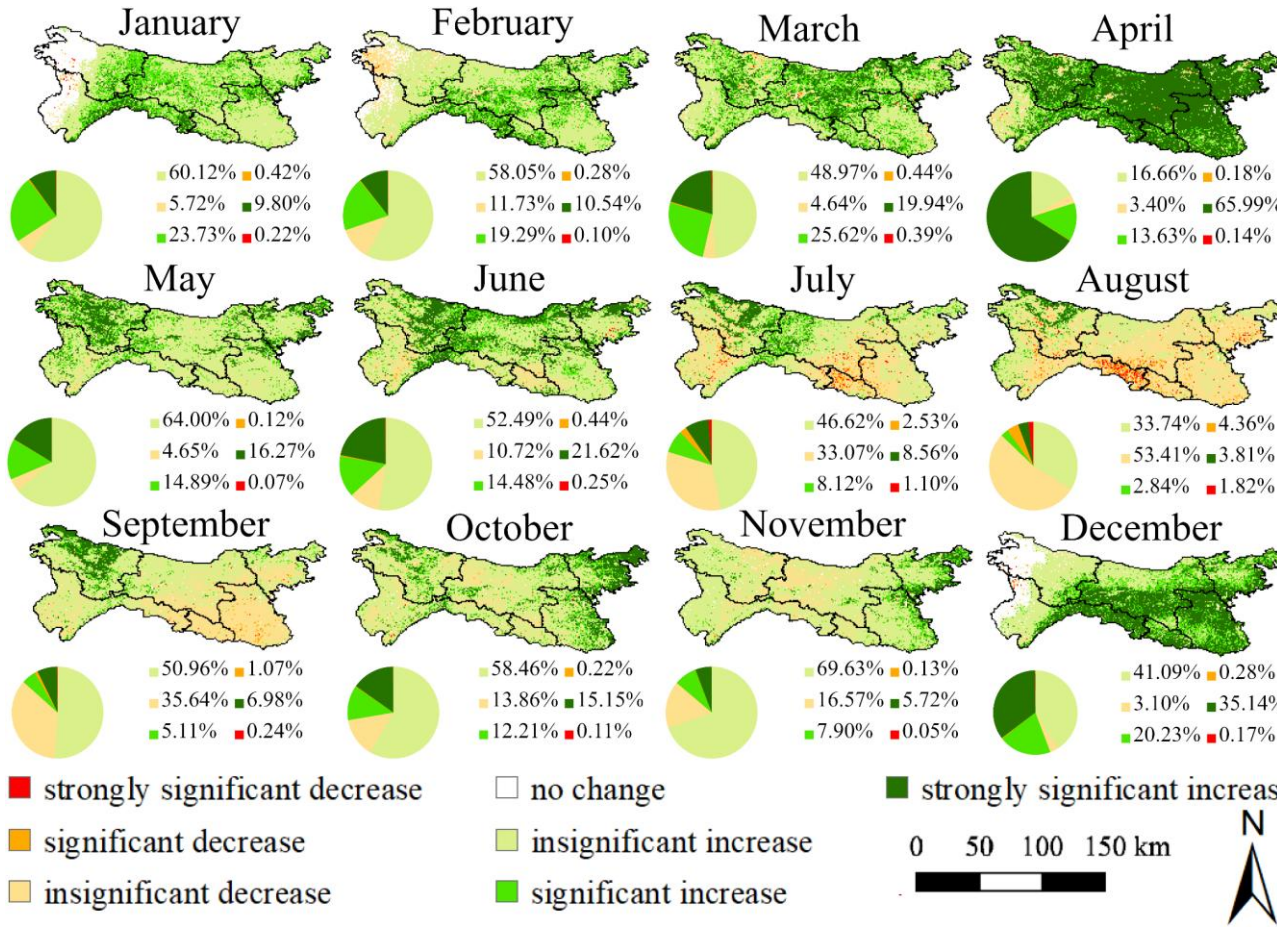


Figure 6. Spatial trends in vegetation NPP from January to December during 2001–2024.

4.2 Driving Mechanisms of Vegetation NPP

To investigate the relationship between monthly NPP and environmental factors in the QBMs, the XGBoost-SHAP interpretation method described in Section 3.3 was applied. This method quantified the relative contributions and positive or negative effects of different factors on monthly NPP. It further identified the dominant explanatory factors and their monthly variations.

The validation results of the XGBoost model showed a strong consistency between observed and predicted values across all months (Figure 7). Most samples were distributed close to the trend line, with R^2 values ranging from 0.68 to 0.90 and RMSE values ranging from 1.95 to 18.69. The model achieved the highest accuracy in January (R^2 = 0.90, RMSE = 1.95), whereas the lowest R^2 was observed in August (0.68). The highest RMSE occurred in July (18.69), indicating monthly differences in model performance.

SHAP analysis revealed clear monthly variations and shifts in the dominant explanatory factors of NPP (Figure 8). From December to February, Tsoil and Rad were the main contributors. In February, Rad became the dominant factor, with a contribution of 43.3%, exceeding Tsoil (23.0%). The contribution of Pre also increased to 9.0%. From

March to May, Rad remained dominant, although its contribution gradually declined from 47.5% to 31.6%.

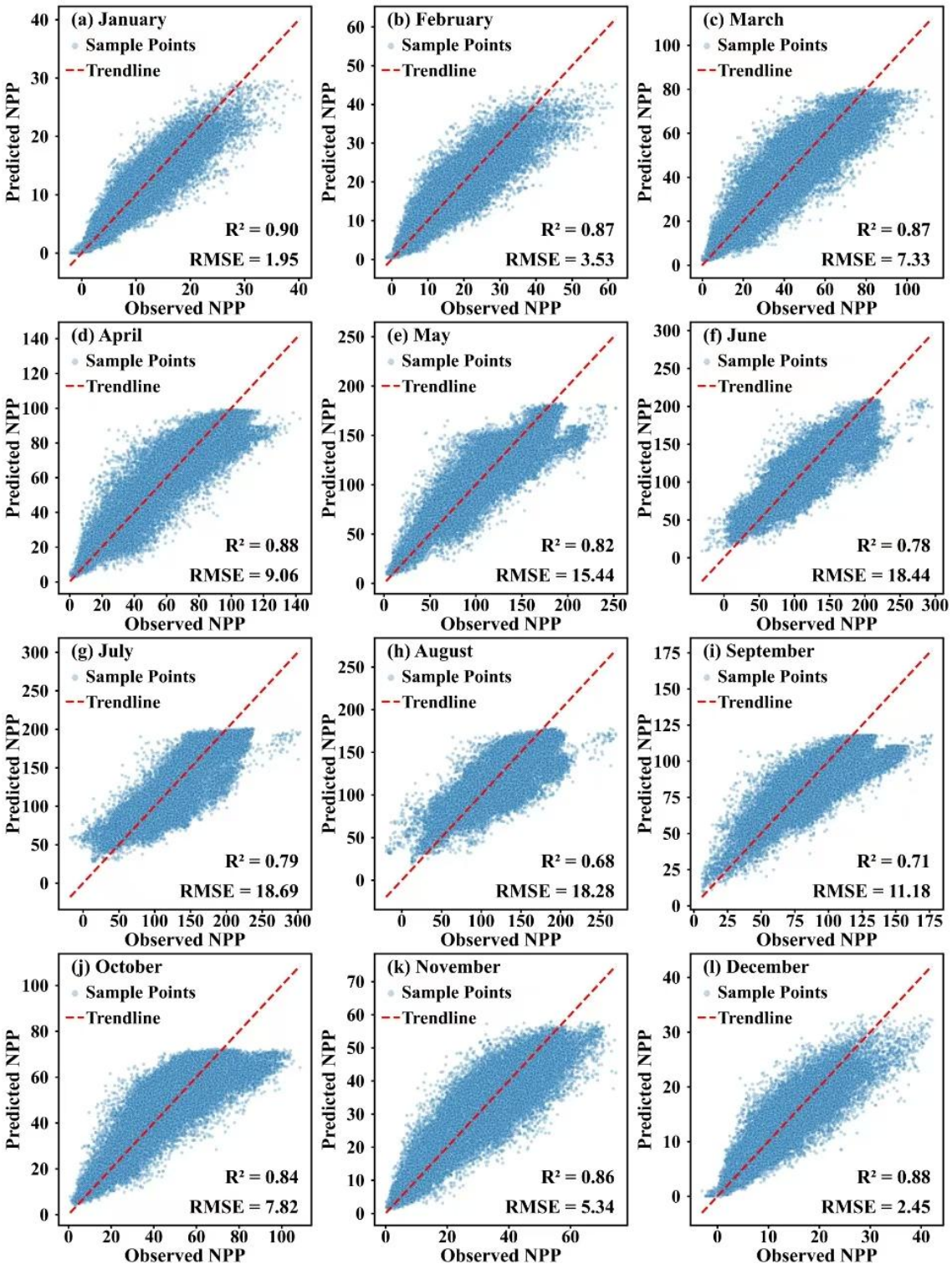


Figure 7. Scatter plots of observed versus predicted NPP values: panels (a)–(l) correspond to the fitting results from January to December, respectively. Blue points represent sample points, while the red dashed line indicates the fitted linear trend. R^2 and RMSE indicate model goodness of fit and prediction error, respectively.

Meanwhile, the contributions of Pre, Tsoil, and Tem increased, indicating a transition toward multiple-factor regulation. From June to August, Tsoil regained dominance, with contributions close to 50%. Its effect direction changed from positive to negative in June. Pre increased markedly, reaching 20.8% in July and remaining higher than Rad in August (13.9% vs. 9.1%), making it the second most important factor during July–August. From

September to November, the dominant factors shifted again. Pre and LC showed the highest contributions in September (19.4% and 17.7%, respectively). By November, Rad became dominant again, with a contribution of 29.1%, exceeding Tsoil (18.7%) and Pre (17.5%).

Overall, Tsoil, Rad, and Pre were the dominant explanatory factors for monthly NPP variations in the QBMs, whereas SM, DEM, Slope, and Aspect showed relatively low contributions. The contribution of Tem exhibited clear monthly fluctuations, with higher importance in April–May, relatively stable contributions during June–August, and an increasing trend again in October–November. Based on the monthly variations in explanatory factors, February, June, September, and November were identified as key transition points in the monthly NPP explanatory patterns. These transitions corresponded to the shift from Tsoil dominance to Rad dominance in February, the change of Tsoil effects from positive to negative accompanied by increased Pre contribution in June, the enhanced contributions of Pre and LC in September, and the re-establishment of Rad as the dominant factor in November.

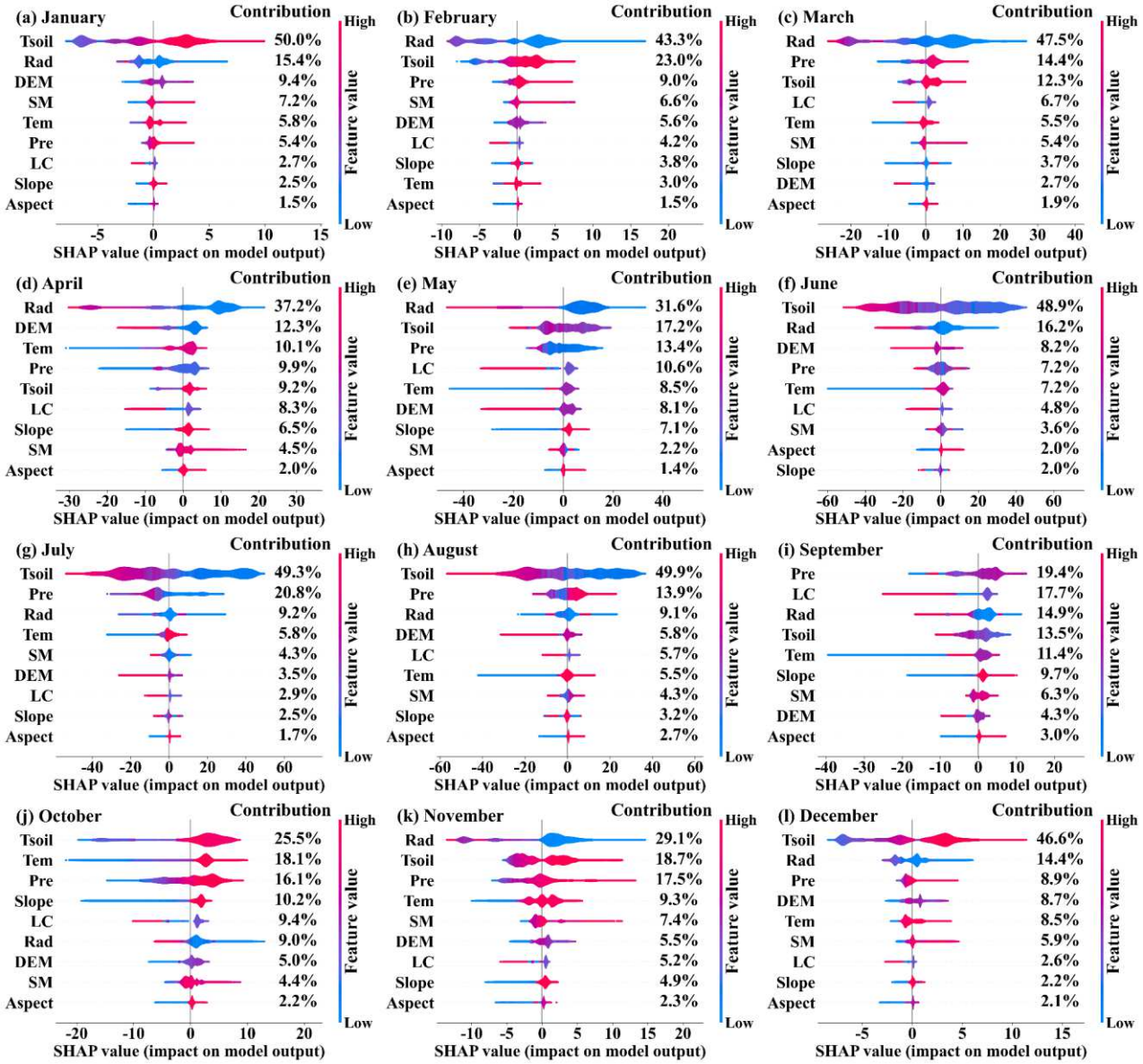


Figure 8. SHAP-based impact analysis of vegetation NPP in the QBMs across different months: panels (a)–(l) correspond to the SHAP results for January to December.

4.3 Lagged and Cumulative Responses of Vegetation NPP to Climate

To further examine the lag and cumulative effects of climatic factors on vegetation NPP in the QBMs, the

cumulative and lag effect analysis described in Section 3.4 was applied. The results indicated that the lag and cumulative effects of different climatic factors on NPP exhibited pronounced spatial heterogeneity (Figure 9, Table 3).

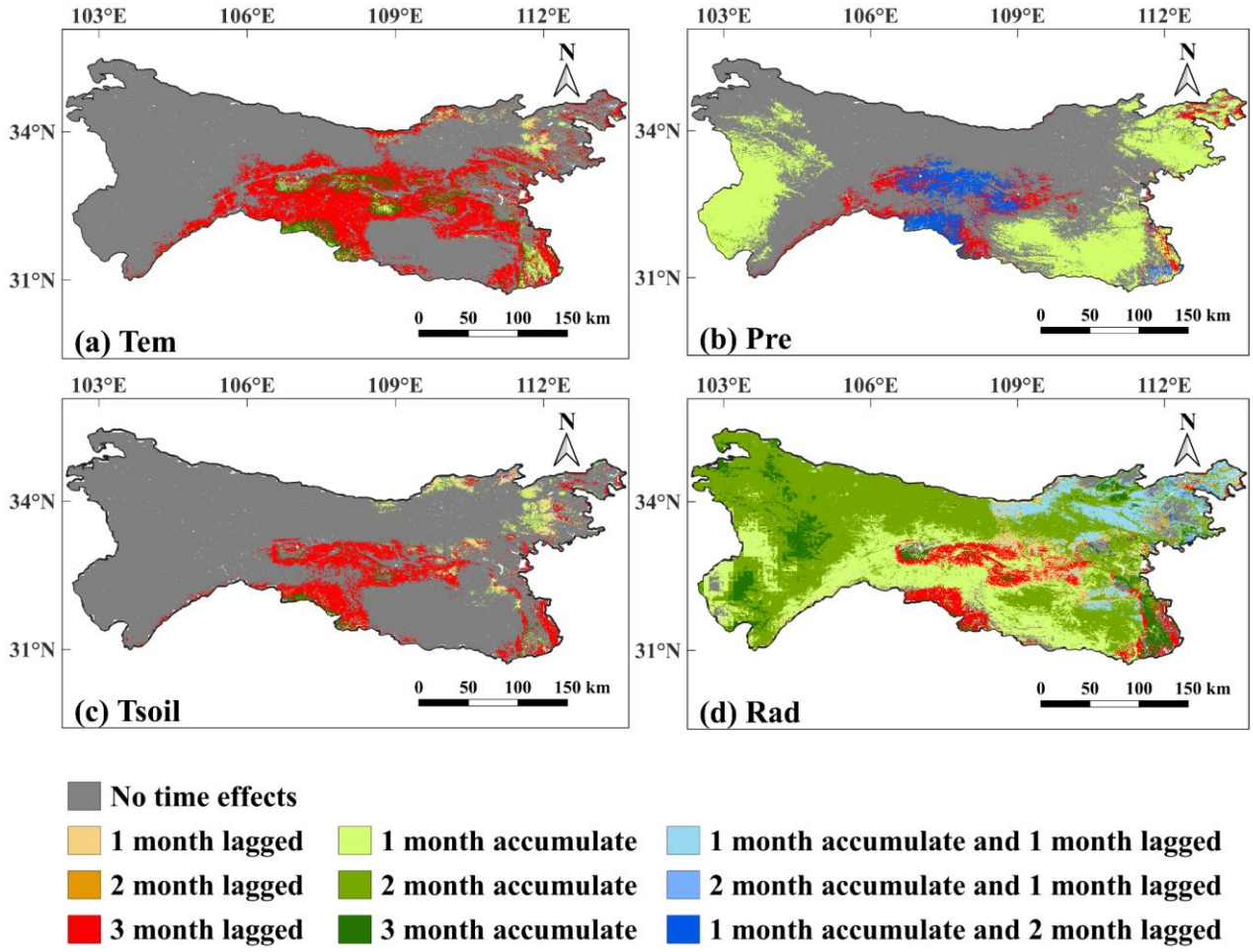


Figure 9. Spatial distribution of lagged and cumulative response types of vegetation NPP to different climatic factors: panels (a)-(d) correspond to temperature, precipitation, soil temperature, and solar radiation

Table 3. Proportions of different lagged and cumulative response types of vegetation NPP to climatic factors.

Type	Tem (%)	Pre (%)	Tsoil (%)	Rad (%)
L0A0	72.54	62.41	85.75	3.95
L0A1	2.00	26.49	1.91	22.84
L0A2	0.95	0.25	0.03	46.93
L0A3	2.82	0.10	0.68	6.81
L1A0	0.52	0.01	1.23	3.40
L1A1	0.00	0.09	0.07	7.75
L1A2	0.01	0.17	0.07	0.70
L2A0	0.01	0.01	0.06	0.68
L2A1	0.12	5.12	0.06	0.26
L3A0	21.02	5.35	10.14	6.68

Note: L and A denote lag time and accumulation time, respectively, both in months. L0A0 represents no obvious lagged or cumulative effect; L0A1–L0A3 represent 1–3-month cumulative effects; L1A0–L3A0 represent 1–3-month lagged effects; and L1A1, L1A2, and L2A1 represent compound lagged–cumulative effects.

For Tem, most areas showed no temporal effect (72.54%). Among the areas with detectable temporal effects,

the 3-month lag effect was dominant (21.02%), mainly occurring around the Ankang Basin, the Nanyang Basin, the Taibai Mountain area, and the southeastern part of the study area. Tsoil showed a higher proportion of areas with no temporal effect (85.75%). In areas where temporal effects were detected, the 3-month lag effect remained dominant, mainly occurring in the central-southern part of the study area and extending toward the southern and southeastern regions. For Pre, most areas also exhibited no temporal effect (62.41%). Among the areas with detectable temporal effects, the 1-month cumulative effect was the most prominent (26.49%), primarily distributed in the Minshan Mountains in the western part of the study area, the northeastern plains, and the Shennongjia region in the southeast. The 3-month lag effect (5.35%) and the combined 1-month cumulative and 2-month lag effect (5.12%) were less extensive. Rad exhibited a pronounced cumulative effect. The 2-month cumulative effect was dominant (46.93%), mainly distributed in the western part of the study area, the northern Qinling Mountains, and most central-eastern regions. The 1-month cumulative effect was the second most important pattern (22.84%), primarily occurring in the central-southern region. In contrast, lag effects and no temporal effect accounted for relatively small proportions (6.68% and 3.95%, respectively).

Overall, Tem and Tsoil were mainly characterized by no time effects and 3-month lag effects. Pre was dominated by no time effects and 1-month cumulative effects, whereas Rad showed a predominant 2-month cumulative effect. Spatially, the 3-month lag effects were mainly distributed in the Hanjiang Basin, Ankang Basin, and surrounding areas, while cumulative effects were more evident in the western, northern, and central-eastern regions of the QBMs.

5. Discussion

5.1 Spatiotemporal Dynamics of Monthly Vegetation NPP

Over recent decades, approximately one-third of global vegetated areas have experienced significant greening and increased vegetation productivity. This trend is particularly evident in mid- and high-latitude regions of the Northern Hemisphere. It is especially pronounced in temperate and boreal ecosystems[51-53]. Vegetation in these regions is typically subject to strong temperature limitation and is therefore highly sensitive to climate warming[54,55]. In this study, monthly vegetation NPP in the QBMs exhibited an overall increasing trend during 2001–2024 (Figure 3), which is broadly consistent with previous findings [51,53,55]. However, annual-scale analyses mainly capture overall temporal trends and provide limited insight into the relative contributions of individual months to long-term NPP increases. Our results further showed that NPP increases in the QBMs from 2001 to 2024 occurred primarily in April and May, with additional increases observed in low-NPP months such as December and January (Figure 4). This temporal pattern is likely associated with weakened low-temperature limitation in late winter and early spring under climate warming, as well as an earlier onset of the growing season[54-56]. Improved temperature conditions during the cold season and early spring may alleviate low-temperature constraints on vegetation physiological activity. This enables vegetation to resume growth earlier after winter dormancy. As a result, NPP increases during months with relatively low productivity. In addition, more favorable heat and radiation conditions in early spring may facilitate vegetation green-up, leaf expansion, and the initiation of photosynthetic activity, leading to a rapid increase in NPP during April and May[56,57]. Zhu and Lu[58] reported that vegetation phenology in the QBMs responds significantly to climate change, with an advance in the start of the growing season being a key manifestation of regional phenological change. This finding is consistent with the pronounced NPP increase observed in April and May. It suggests that enhanced spring NPP in the QBMs may be closely related to earlier vegetation growth initiation and strengthened photosynthetic activity during the early growing season[56-58]. Previous studies have also shown that phenological shifts can substantially affect vegetation productivity, and that an earlier start of the growing season generally enhances spring carbon uptake capacity[56,57]. Therefore, the long-term increase in monthly NPP in the QBMs may result from the combined effects of weakened cold-season temperature limitation, advanced spring phenology, and enhanced photosynthetic capacity during the early growing season.

In complex mountainous ecosystems, vegetation responses to climate change are jointly regulated by elevation, aspect, and geomorphic setting. The redistribution of thermal and moisture conditions across different topographic positions can generate pronounced spatial non-stationarity[59-61]. Such non-stationarity is reflected not only in the spatial distribution of high and low NPP values, but also in asynchronous timing among regions in entering the growing season, reaching peak productivity, and initiating seasonal decline[24,60,61]. In this study, the spatial pattern of monthly NPP in the QBMs showed a pronounced process of spatial advancement and retreat across months. During the early growing season, NPP increased first in low-elevation areas along the Hanjiang River and on the southern slope of the Daba Mountains. During the peak growing season, the productivity advantage shifted toward higher-elevation areas, whereas in the late growing season, NPP declined first in the western high-elevation regions. This spatial asynchrony may be closely associated with the spatial differentiation of vegetation phenology[24,60,61]. Zhu and Lu[58] reported that vegetation along the Hanjiang River and on the southern slope of the Daba Mountains was generally characterized by an earlier growing-season onset, delayed senescence, and a longer growing-season duration, whereas high-elevation areas, such as the western Qinling Mountains, exhibited a delayed onset, earlier termination, and shorter growing season. Li et al[24] further demonstrated that spring phenology in the QBMs varies systematically along elevation gradients, with the start of the growing season occurring earlier in valley areas and later in mountainous regions. These phenological gradients are broadly consistent with the spatial advancement and retreat of monthly NPP identified in this study.

In addition, the long-term increase in NPP during the summer peak period was relatively limited, suggesting that high productivity does not necessarily imply a continued potential for further enhancement in this study. Recent studies have reported an increase in summer extreme heat events and atmospheric evaporative demand in parts of central and eastern China. These changes may intensify vegetation water stress. As a result, further improvements in summer photosynthetic potential may be constrained[62,63]. In the QBMs, vegetation growth in low-elevation basins and plains tends to start earlier in spring. However, these areas are more vulnerable to the combined effects of high temperature, enhanced evapotranspiration, and insufficient water supply during summer. These conditions may limit further increases in NPP during the peak productivity period[64]. This interpretation is supported by the driving mechanism analysis. The XGBoost–SHAP results showed that June represented a key transition point in the NPP driving mechanism in the QBMs (Figure 8). Specifically, the effect of Tsoil on NPP shifted from positive in the preceding months to negative in June, while the relative importance of Pre continued to increase and surpassed that of Rad in July–August. These results suggest that, after the onset of summer, thermal conditions may shift from a favorable factor promoting vegetation growth in spring to a potential stressor constraining further NPP enhancement. At the same time, water supply becomes increasingly important for maintaining the stability of summer NPP.

5.2 Shifts in the Driving Mechanisms of Monthly Vegetation NPP

The XGBoost–SHAP analysis revealed a clear monthly succession of dominant drivers. The system shifted from thermal and radiation constraints during December to February of the following year. It then transitioned to hydrothermal co-regulation during March–May. Water limitation dominated during June–August. Finally, thermal and radiation control regained dominance during September–November. This dynamic pattern contrasts with traditional annual-scale studies, which often classify a region statically as either temperature-limited or water-limited. Our results suggest that the QBMs, as an ecological transition zone, undergo alternating limiting mechanisms within a single year. The dominance of Tsoil and Rad from December to February of the following year is consistent with the recognized role of thermal limitation during the dormant season[57,65]. The February transition, when Rad surpassed Tsoil, suggests that light availability becomes increasingly important as vegetation approaches the growing season, providing useful implications for predicting spring phenological responses under climate change. The shift toward hydrothermal co-regulation during March–May reflects the co-limitation characteristics of temperate ecosystems. The increasing importance of Pre and SM during this period indicates that water availability may begin to constrain vegetation growth even before summer, particularly under warming conditions[66]. The transition toward water limitation during June–August was particularly evident. During this period, Pre surpassed Rad as a dominant

factor, while the effect of Tsoil shifted from positive to negative. This finding is consistent with previous evidence that high temperatures can intensify evapotranspiration and water stress, thereby suppressing NPP. The negative effect of summer Tsoil further suggests that excessive warming may aggravate water deficits, consistent with observations from arid and semi-arid regions[64]. In September, Pre and LC became dominant drivers. In October–November, thermal and radiation control re-emerged. These patterns indicate that the termination of the growing season is jointly regulated by water conditions and vegetation type differences. Thermal limitation becomes dominant again as winter approaches[66,67].

5.3 Differential Responses of Vegetation NPP to the Lagged and Cumulative Effects of Climatic Factors

This study highlights the temporal effects of climatic factors on vegetation NPP. Different climatic factors can influence vegetation growth over different time scales, reflecting both the sensitivity of vegetation to climate change and the dynamic nature of its responses[48,68]. Although vegetation can adapt to climatic variability within a certain range, growth may be suppressed or even cease when climate change exceeds critical thresholds[69]. Therefore, vegetation responses to climate are not necessarily instantaneous; instead, climatic effects may influence subsequent vegetation growth through lagged or cumulative pathways[20,22,70].

This study investigated the lagged and cumulative effects of climatic factors on vegetation NPP in the QBMs at the pixel scale. The results indicated that vegetation dynamics in the QBMs were influenced by both concurrent climatic conditions and antecedent climate signals (Figure 9a, c). Previous studies of global vegetation dynamics have suggested that vegetation responses to temperature are generally more immediate[48], which is broadly consistent with our findings. However, beyond this generally direct temperature response, our results further revealed pronounced 3-month lag effects of Tem and Tsoil in parts of the Hanjiang Basin, the Nanyang Basin, and their surrounding areas. This difference may be related to the hydrothermal buffering effects of basin topography and relatively thick soil layers. In such environments, antecedent temperature may influence later vegetation productivity by affecting phenological onset, root activity, soil microbial processes, and nutrient release[71,72.]

Compared with the lagged responses to Tem and Tsoil, Pre and Rad exhibited pronounced cumulative effects. For Pre, the 1-month cumulative effect was the most prominent, which is consistent with the findings of Ding et al[48]. Moreover, this study further showed that the cumulative effect of Pre was stronger than its lag effect in several regions, including the Minshan Mountains in the western QBMs, the northeastern plains, and Shennongjia in the southeast. This suggests that antecedent precipitation can exert a sustained influence on vegetation growth in the study area, consistent with the findings of Liu et al[68]. Vegetation generally does not respond directly to precipitation itself, but rather to the actual availability of soil water[73]. This is because increased precipitation cannot be immediately absorbed and utilized by vegetation; instead, water requires time to infiltrate into the root zone[74]. In addition, the upward replenishment of deep soil water also occurs with a time delay. When short-term rainfall exceeds plant water-use capacity, soils can retain part of the surplus water, thereby providing a longer-lasting water supply and sustaining vegetation growth in subsequent periods[75]. Ding et al[48] further demonstrated that, across most regions, the cumulative effect of precipitation is generally stronger than its lag effect, regardless of climatic zone or vegetation type. This evidence supports the view that cumulative water availability over a given time interval plays a more substantial role in vegetation growth than instantaneous water availability at a single time point.

The cumulative effect of Rad is also consistent with previous evidence that sustained light-energy supply can regulate vegetation growth. Rad affects contemporaneous photosynthesis, while also influencing subsequent productivity through the regulation of canopy development, leaf area expansion, and carbon assimilation capacity[4,76]. In this study, Rad was mainly characterized by cumulative effects over relatively long time scales, indicating that vegetation NPP in the QBMs responds continuously to light-energy conditions. Moreover, the cumulative effect of Rad exhibited clear aspect-related differences in the QBMs (Figure 9d). The northern slopes were mainly dominated by a 2-month cumulative effect, whereas the southern slopes were primarily characterized by a 1-month cumulative effect. This pattern is consistent with previous findings that accumulated light-energy supply can exert

sustained effects on vegetation productivity[22,48], while also highlighting the regulatory role of topography. This difference may be attributed to the relatively weaker light and thermal conditions on northern slopes. These conditions are mainly caused by aspect effects and terrain shading. Under such conditions, vegetation responses to Rad may require a longer accumulation period before becoming fully apparent[19,49,77,78]. By contrast, southern slopes generally receive more favorable light conditions, allowing Rad to contribute more rapidly to photosynthesis and carbon accumulation and thereby affect NPP over a shorter time scale[79,80]. These results suggest that the cumulative effect of Rad in the QBMs arises from the continuity of antecedent light-energy supply as well as the joint regulation of aspect, topographic conditions, and vegetation growth processes.

5.4 Limitations, and future directions

This study has several limitations. First, although the MODIS NPP product has been widely validated, satellite-derived NPP estimates still contain uncertainties. In mountainous regions such as the QBMs, complex topography and strong spatial heterogeneity may introduce additional uncertainties and affect NPP trend estimation. Second, although LC was included to represent anthropogenic influences, it cannot fully capture detailed human activities, such as grazing intensity, forest management, and ecological conservation practices. Future studies should integrate multi-source human activity datasets to better quantify the effects of anthropogenic factors on NPP dynamics. Third, this study mainly considered climatic and topographic factors, while other potential drivers, including atmospheric CO_2 concentration, nutrient availability, and extreme climate events, were not included. In addition, the XGBoost-SHAP framework mainly reveals statistical associations rather than causal relationships. Future research should combine multi-source environmental data, field observations, and process-based ecosystem models to further improve the understanding of mechanisms controlling NPP variations.

6. Conclusions

Using MODIS NPP data and multi-source environmental datasets from 2001 to 2024, this study investigated the spatiotemporal dynamics and driving mechanisms of monthly vegetation NPP in the QBMs. Monthly NPP exhibited a stable seasonal cycle and a persistent upward trend. Spatially, monthly NPP showed distinct stage-dependent reorganization, shifting from a northwest-low and southeast-high pattern to a northwest-high and southeast-low pattern before gradually returning to the initial configuration. The dominant drivers of monthly NPP changed markedly throughout the year, with February, June, September, and November representing key transition points. Solar radiation exceeded soil temperature in February. Soil temperature shifted from positive to negative in June, with increased precipitation contribution. Precipitation and land cover strengthened in September. And solar radiation regained dominance in November. In addition, vegetation NPP exhibited clear cumulative and lagged responses to climatic factors, with temperature mainly showing a 3-month lag effect, Precipitation a 1-month cumulative effect, and solar radiation a 2-month cumulative effect.

Overall, the findings of this study emphasize the importance of understanding the dynamic mechanisms of monthly NPP variations and their responses to climatic factors in the Qinba Mountains. This approach provides insights into vegetation–climate interactions and the temporal responses of vegetation productivity to environmental changes, contributing to a better understanding of ecosystem processes in complex mountainous regions.

References

1 Friedlingstein, P. *et al.* Global carbon budget 2025. *Earth Syst. Sci. Data* **18**, 3211–3288 (2026).

2 Bonan, G. B. Forests and climate change: forcings, feedbacks, and the climate benefits of forests. *Science* **320**, 1444–1449 (2008).

3 Field, C. B., Behrenfeld, M. J., Randerson, J. T. & Falkowski, P. Primary production of the biosphere: integrating terrestrial and oceanic components. *Science* **281**, 237–240 (1998).

4 Running, S. W. *et al.* A continuous satellite-derived measure of global terrestrial primary production.

BioScience **54**, 547–560 (2004).

5 Roxburgh, S. H., Berry, S. L., Buckley, T. N., Barnes, B. & Roderick, M. L. What is NPP? Inconsistent accounting of respiratory fluxes in the definition of net primary production. *Funct. Ecol.* **19**, 378–382 (2005).

6 Kooistra, L. *et al.* Reviews and syntheses: Remotely sensed optical time series for monitoring vegetation productivity. *Biogeosciences* **21**, 473–511 (2024).

7 Hazarika, M. K., Yasuoka, Y., Ito, A. & Dye, D. Estimation of net primary productivity by integrating remote sensing data with an ecosystem model. *Remote Sens. Environ.* **94**, 298–310 (2005).

8 Park, E. *et al.* Advancement of a diagnostic prediction model for spatiotemporal calibration of earth observation data: a case study on projecting forest net primary production in the mid-latitude region. *GISci. Remote Sens.* **61**, 2401247 (2024).

9 Liang, W. *et al.* Analysis of spatial and temporal patterns of net primary production and their climate controls in China from 1982 to 2010. *Agric. For. Meteorol.* **204**, 22–36 (2015).

10 Ge, W., Deng, L., Wang, F. & Han, J. Quantifying the contributions of human activities and climate change to vegetation net primary productivity dynamics in China from 2001 to 2016. *Sci. Total Environ.* **773**, 145648 (2021).

11 Liu, Y. *et al.* Grassland dynamics in responses to climate variation and human activities in China from 2000 to 2013. *Sci. Total Environ.* **690**, 27–39 (2019).

12 Xuan, W. & Rao, L. Spatiotemporal dynamics of net primary productivity and its influencing factors in the middle reaches of the Yellow River from 2000 to 2020. *Front. Plant Sci.* **14**, 1043807 (2023).

13 Liu, Y. *et al.* Evaluating the dynamics of grassland net primary productivity in response to climate change in China. *Glob. Ecol. Conserv.* **28**, e01574 (2021).

14 Ma, R. *et al.* Spatiotemporal change of net primary productivity and its response to climate change in temperate grasslands of China. *Front. Plant Sci.* **13**, 899800 (2022).

15 Han, H. *et al.* Seasonal responses of net primary productivity of vegetation to phenological dynamics in the Loess Plateau, China. *Chin. Geogr. Sci.* **32**, 340–357 (2022).

16 Lv, G. *et al.* Disentangling the influential factors driving NPP decrease in Shandong Province: an analysis from time series evaluation using MODIS and CASA model. *Remote Sens.* **16**, 1966 (2024).

17 Song, X. *et al.* Divergent responses of NPP to climate factors among forest types at interannual and inter-monthly scales: an empirical study on four typical forest types in subtropical China. *Forests* **14**, 1474 (2023).

18 Wang, Y., Dai, E. & Wu, C. Spatiotemporal heterogeneity of net primary productivity and response to climate change in the mountain regions of southwest China. *Ecol. Indic.* **132**, 108273 (2021).

19 Wu, D. *et al.* Time-lag effects of global vegetation responses to climate change. *Glob. Change Biol.* **21**, 3520–3531 (2015).

20 Li, C. *et al.* Considering time-lag effects can improve the accuracy of NPP simulation using a light use efficiency model. *J. Geogr. Sci.* **33**, 961–979 (2023).

21 Liu, X. *et al.* Time-lag effect of climate conditions on vegetation productivity in a temperate forest–grassland ecotone. *Forests* **13**, 1024 (2022).

22 Liu, H. *et al.* Analysis of the time-lag effects of climate factors on grassland productivity in Inner Mongolia. *Glob. Ecol. Conserv.* **30**, e01751 (2021).

23 Liu, X. *et al.* Vegetation dynamics in Qinling-Daba Mountains in relation to climate factors between 2000 and 2014. *J. Geogr. Sci.* **26**, 45–58 (2016).

24 Li, J. *et al.* Important role of precipitation in controlling a more uniform spring phenology in the Qinba Mountains, China. *Front. Plant Sci.* **14**, 1074405 (2023).

25 Zhou, Y., Liu, H., Zhao, Z. & Yang, R. Spatial system of national parks and protected areas in Qinba Mountain Area. *Strategic Study of CAE* **22**, 86–95 (2020).

26 Li, J., Liu, S., Peng, B., Ye, H. & Zhang, Z. Identification and optimization of county-level ecological spaces

under the dual-carbon target: a case study of Shaanxi Province, China. *Remote Sens.* **15**, 4009 (2023).
27 He, T. *et al.* Response of net primary productivity of vegetation to drought: a case study of Qinba Mountainous area, China (2001–2018). *Ecol. Indic.* **149**, 110148 (2023).
28 Zeng, Q. & Hao, C. Response of vegetation net primary productivity to extreme climate in a climate transition zone: evidence from the Qinling Mountains. *Atmosphere* **16**, 1208 (2025).
29 Lan, X. *et al.* Spatiotemporal variation of climate of different flanks and elevations of the Qinling–Daba mountains in China during 1969–2018. *Sci. Rep.* **12**, 6952 (2022).
30 Jiang, Y., Zhang, B., Yao, Y., Li, J. & Liu, J. Effects of the Qinling–Daba Mountains as ecological corridor on patterns of plant distribution. *Ecol. Evol.* **15**, e71633 (2025).
31 Yu, F. *et al.* Identifying connectivity conservation priorities among protected areas in Qinling–Daba Mountains, China. *Sustainability* **14**, 4377 (2022).
32 Yao, Y. Pattern and change of NDVI and their environmental influencing factors for 1986–2019 in the Qinling–Daba Mountains of central China. *Front. For. Glob. Change* **7**, 1372488 (2024).
33 Zhang, X. *et al.* A database of seed plants on taxonomy, geography and ecology in the Qinling–Daba Mountains and adjacent areas. *Sci. Data* **9**, 672 (2022).
34 Liu, J. *et al.* Latitudinal differentiation and patterns of temperate and subtropical plants in the Qinling–Daba Mountains. *J. Geogr. Sci.* **33**, 907–923 (2023).
35 Zhao, F., Liu, J., Zhu, W., Zhang, B. & Zhu, L. Spatial variation of altitudinal belts as dividing index between warm temperate and subtropical zones in the Qinling–Daba Mountains. *J. Geogr. Sci.* **30**, 642–656 (2020).
36 Cleveland, R. B., Cleveland, W. S., McRae, J. E. & Terpenning, I. STL: a seasonal-trend decomposition procedure based on loess. *J. Off. Stat.* **6**, 3–73 (1990).
37 Wen, Q. *et al.* RobustSTL: a robust seasonal-trend decomposition algorithm for long time series. *Proc. AAAI Conf. Artif. Intell*. **33**, 5409–5416 (2019).
38 Cleveland, W. S. & Devlin, S. J. Locally weighted regression: an approach to regression analysis by local fitting. *J. Am. Stat. Assoc.* **83**, 596–610 (1988).
39 Wang, X. C., Smith, K. A. & Hyndman, R. J. Characteristic-based clustering for time series data. *Data Min. Knowl. Discov.* **13**, 335–364 (2006).
40 Kang, Y., Hyndman, R. J. & Smith-Miles, K. Visualising forecasting algorithm performance using time series instance spaces. *Int. J. Forecast.* 33, 345–358 (2017).
41 Theil, H. A rank-invariant method of linear and polynomial regression analysis. *Indag. Math.* **12**, 173 (1950).
42 Sen, P. K. Estimates of the regression coefficient based on Kendall's tau. *J. Am. Stat. Assoc.* **63**, 1379–1389 (1968).
43 Mann, H. B. Nonparametric tests against trend. *Econometrica* **13**, 245–259 (1945).
44 Kendall, M. G. A new measure of rank correlation. *Biometrika* **30**, 81–93 (1938).
45 Hirsch, R. M., Slack, J. R. & Smith, R. A. Techniques of trend analysis for monthly water quality data. *Water Resour. Res.* **18**, 107–121 (1982).
46 Chen, T. & Guestrin, C. XGBoost: a scalable tree boosting system. *In Proceedings of the 22nd AC M SIGKDD International Conference on Knowledge Discovery and Data Mining* 785–794 (ACM, 20 16). https://doi.org/10.1145/2939672.2939785.
47 Lundberg, S. M. & Lee, S.-I. A unified approach to interpreting model predictions. *Adv. Neural Inf. Process. Syst.* **30**, 4768–4777 (2017).
48 Ding, Y., Li, Z. & Peng, S. Global analysis of time-lag and-accumulation effects of climate on vegetation growth. *Int. J. Appl. Earth Obs. Geoinf.* **92**, 102179 (2020).
49 Wen, Y. *et al.* Cumulative effects of climatic factors on terrestrial vegetation growth. *J. Geophys. Res: Biogeosci.* **124**, 789–806 (2019).
50 Li, N. & Wang, D. Quantifying time-lag and time-accumulation effects of climate change and human activities

on vegetation dynamics in the Yarlung Zangbo River Basin of the Tibetan Plateau. *Remote Sens.* **17**, 160 (2025).
51 Zhu, Z. *et al.* Greening of the Earth and its drivers. *Nat. Clim. Chang.* **6**, 791–795 (2016).
52 Chen, C. *et al.* China and India lead in greening of the world through land-use management. *Nat. Sustain.* **2**, 122–129 (2019).
53 Piao, S. *et al.* Characteristics, drivers and feedbacks of global greening. *Nat. Rev. Earth Environ.* **1**, 14–27 (2020).
54 Piao, S. *et al.* Weakening temperature control on the interannual variations of spring carbon uptake across northern lands. *Nat. Clim. Chang.* **7**, 359–363 (2017).
55 Zhang, Y. *et al.* Future reversal of warming-enhanced vegetation productivity in the Northern Hemisphere. *Nat. Clim. Chang.* **12**, 581–586 (2022).
56 Gu, H. *et al.* Warming-induced increase in carbon uptake is linked to earlier spring phenology in temperate and boreal forests. *Nat. Commun*. **13**, 3698 (2022).
57 Richardson, A. D. *et al.* Climate change, phenology, and phenological control of vegetation feedbacks to the climate system. *Agric. For. Meteorol.* **169**, 156–173 (2013).
58 Zhu, W. & Lu, Y. Spatio-temporal patterns and climatic drivers of spring phenology in eight forest communities across the north-south transitional zone of China. *J. Geogr. Sci.* **35**, 17–38 (2025).
59 Wang, X. *et al.* Detecting spatially non-stationary between vegetation and related factors in the Yellow River Basin from 1986 to 2021 using multiscale geographically weighted regression based on Landsat. *Remote Sens.* **14**, 6276 (2022).
60 Deng, C., Ma, X., Xie, M. & Bai, H. Effect of altitude and topography on vegetation phenological changes in the Niubeiliang nature reserve of Qinling Mountains, China. *Forests* **13**, 1229 (2022).
61 Ding, C., Li, Y., Xie, Q., Li, H. & Zhang, B. Impacts of terrain on land surface phenology derived from Harmonized Landsat 8 and Sentinel-2 in the Tianshan Mountains, China. *GISci. Remote Sens.* **60**, 2242621 (2023).
62 Wang, F., Gao, M., Liu, C., Zhao, R. & McElroy, M. B. Uniformly elevated future heat stress in China driven by spatially heterogeneous water vapor changes. *Nat. Commun.* **15**, 4522 (2024).
63 Yuan, W. *et al.* Increased atmospheric vapor pressure deficit reduces global vegetation growth. *Sci. Adv.* **5**, eaax1396 (2019).
64 Qi, G. *et al.* Soil moisture plays an increasingly important role in constraining vegetation productivity in China over the past two decades. *Agric. For. Meteorol.* **356**, 110193 (2024).
65 Stettz, S. G. *et al.* Resolving temperature limitation on spring productivity in an evergreen conifer forest using a model-data fusion framework. *Biogeosciences* **19**, 541–558 (2022).
66 Wang, Q. *et al.* Understanding vegetation phenology responses to easily ignored climate factors in china's mid-high latitudes. *Sci. Rep.* **14**, 8773 (2024).
67 Du, H. *et al.* Responses of autumn vegetation phenology to climate change and urbanization at northern middle and high latitudes. *Int. J. Appl. Earth Obs. Geoinf.* **115**, 103086 (2022).
68 Liu, M. *et al.* Time-lag and accumulation responses of vegetation growth to average and extreme precipitation and temperature events in China between 2001 and 2020. *Sci. Total Environ.* **945**, 174084 (2024).
69 Li, X. *et al.* Global variations in critical drought thresholds that impact vegetation. *Natl. Sci. Rev.* **10**, nwad049 (2023).
70 Shi, S., Wang, P., Zhang, Y. & Yu, J. Cumulative and time-lag effects of the main climate factors on natural vegetation across Siberia. *Ecol. Indic.* **133**, 108446 (2021).
71 Pregitzer, K. S. & King, J. S. Effects of soil temperature on nutrient uptake in *Nutrient Acquisition by Plants (*ed. BassiriRad, H.*)* 277–310 (Springer, 2005). https://doi.org/10.1007/3-540-27675-0_10.
72 Van Nuland, M. E. *et al.* Natural soil microbiome variation affects spring foliar phenology with consequences for plant productivity and climate-driven range shifts. *New Phytol.* **232**, 762–775 (2021).

73 Vicente-Serrano, S. M. *et al.* Response of vegetation to drought time-scales across global land biomes. *Proc. Natl. Acad. Sci. USA* **110**, 52–57 (2013).
74 Rodríguez-Iturbe, I. & Porporato, A. M. M. *Ecohydrology of Water-Controlled Ecosystems: Soil Moisture and Plant Dynamics*. (Cambridge University Press, 2005). https://doi.org/10.1017/CBO978051153572.
75 Sala, O. E., Gherardi, L. A., Reichmann, L., Jobbágy, E. & Peters, D. Legacies of precipitation fluctuations on primary production: theory and data synthesis. *Philos. Trans. R. Soc. B Biol. Sci.* **367**, 3135–3144 (2012).
76 Myneni, R. B., Keeling, C., Tucker, C. J., Asrar, G. & Nemani, R. R. Increased plant growth in the northern high latitudes from 1981 to 1991. *Nature* **386**, 698–702 (1997).
77 Bennie, J., Huntley, B., Wiltshire, A., Hill, M. O. & Baxter, R. Slope, aspect and climate: spatially explicit and implicit models of topographic microclimate in chalk grassland. *Ecol. Modell.* **216**, 47–59 (2008).
78 Fu, P. & Rich, P. M. A geometric solar radiation model with applications in agriculture and forestry. *Comput. Electron. Agric.* **37**, 25–35 (2002).
79 Monteith, J. L. Solar radiation and productivity in tropical ecosystems. *J. Appl. Ecol.* **9**, 747–766 (1972).
80 Ruimy, A., Jarvis, P., Baldocchi, D. D. & Saugier, B. CO_2 fluxes over plant canopies and solar radiation: a review. *Adv. Ecol. Res.* **26**, 1–68 (1995).

Author contributions

Conceptualization, F.X. and J.N.; Methodology, F.X. and X.Y.; Software, X.Y. and F.H.; Formal analysis, F.H. and S.N.; Investigation, S.N., L.L. and S.L.; Resources, F.X. and J.N.; Data curation, X.Y. and F.H.; Writing—original draft, F.X.; Writing—review & editing, X.Y., F.H., S.N., L.L., S.L. and J.N.; Visualization, F.H. and L.L.; Supervision, J.N.; Project administration, F.X. and J.N.; Funding acquisition, J.N. All authors have read and agreed to the published version of the manuscript.

Funding

This research was funded by the Natural Science Foundation of Henan Province (No. 252300421290), the National Natural Science Foundation of China (No. 41771438), the Program for Innovative Research Team in Science and Technology of Henan University (No. 22IRTSTHN010), and the Postgraduate Education Reform and Quality Improvement Project of Henan Province (No. HNYJS2020JD14).

Data Availability Statement

The datasets generated and/or analyzed during the current study are not publicly available but are available from the corresponding/first author on reasonable request.

Conflicts of Interest

The authors declare no conflicts of interest.

Consent for Publication

We undertake and agree that the manuscript submitted to your journal has not been published elsewhere and has not been simultaneously submitted to other journals.